NASA

Technical Memorandum 84960

Measurements of Galactic Plane Gamma Ray Emission in the Energy Range from 10 to 80 MeV

D. L. Bertsch and D. A. Kniffen

DECEMBER 1982

National Aeronautics and
Space Administration

Goddard Space Flight Center
Greenbelt, Maryland 20771

MEASUREMENTS OF THE GALACTIC PLANE GAMMA RAY EMISSION IN THE ENERGY RANGE FROM 10 TO 30 MeV

D.L. Bertsch and D.A. Kniffen
NASA/Goddard Space Flight Center
Greenbelt, Maryland 20771

Offprint Request to: D.L. Bertsch, Code 662
NASA/Goddard Space Flight Center
Greenbelt, Maryland 20771, USA

Accepted for publication in the Astrophysical Journal and will appear in the July 1, 1983, issue.

Measurements of Galactic Plane Gamma Ray Emission in the Energy Range from 10 to 80 MeV

D.L. Bertsch and D.A. Kniffen

NASA/Goddard Space Flight Center

ABSTRACT

An improved spark chamber γ-ray telescope has been developed and flown to make measurements of the diffuse galactic γ-ray emission in the important 10 to 80 MeV region. A 24 September 1980 flight was made from Palestine, Texas, to observe the emission from the central region of the galaxy. The extension of observations down to 10 MeV provides important new data indicating that the galactic diffuse γ-ray spectrum continues as a power law down to about 10 MeV, an observation in good agreement with recent theoretical predications. Data from other experiments in the range from 100 keV to 10 MeV show a significant departure from the extension of the power-law fit to the medium energy observations reported here, possibly indicating that a different mechanism may be responsible for the emissions below and above a few MeV. The intensity of the spectrum above 10 MeV implies a galactic electron spectrum which is also very intense down to about 10 MeV. Electrons in this energy range cannot be observed in the solar cavity because of solar modulation effects. The galactic γ-ray data are compared with recent theoretical predictions.

Subject headings: cosmic rays: general-galaxies: Milky Way - galaxies: nuclei - gamma rays: general

I. INTRODUCTION

One of the last regions of the electromagnetic spectrum to be explored is located between high energy x-rays (~ 200 keV) and high energy γ-rays (~ 50 MeV). The principal reason for this is the great difficulty involved in making confident detections of photons at these energies. However, it is generally recognized that the astrophysical information which may be obtained in this energy region is very important, but difficult or even impossible to obtain through observations at other wavelengths.

In the medium energy γ-ray range adopted for this study, 10 to 150 MeV, the contributors to the emission are primarily electromagnetic processes rather than a mixture of many different types of interactions as is the case at lower and higher energies. Hence, this is the optimum energy region for studying the electron component in the source region and the environment in which these energetic electrons reside. This point has been recognized for some time (Fichtel et al., 1976), but because of the observational difficulties, few reliable data yet exist. On the other hand since the region above about 100 MeV is strongly influenced by γ-rays from the decay of neutral pions resulting from the interaction of cosmic ray nucleons with interstellar matter, the comparison with the medium energy γ-rays will address the question of the relative abundance of interstellar electrons and protons, and provide information on the interstellar cosmic ray electron spectrum.

In order to improve the observational capability, a detector system has been developed which takes advantage of the unique signature of the γ-ray pair production processes to make the cleanest possible identification of the ambient γ-rays. A pictoral type detector utilizing digitized spark chambers is combined with a time-of-flight coincidence system to make measurements which are essentially free of instrumental background from the energy range

just above that of nuclear de-exictation lines up to the range where neutral pion decay becomes significant and where many observations already exist.

This paper presents the results of a balloon flight of the new instrument conducted from Palestine, Texas, in September, 1980, to examine the emission from the central region of our galaxy where it is known that there is an enhancement in the high energy emission (Fichtel et al., 1975; Mayer-Hasselwander et al., 1980; Hartman et al., 1979). The results show a surprisingly intense medium energy component, suggesting a greater role for electromagnetic processes than was previously believed to be the case. This may be the result of a very intense interstellar energetic electron component or an enhanced photon density which gives rise to a greater production of Compton scattered γ-rays.

II. SCIENTIFIC BACKGROUND

Shortly following the detailed high energy γ-ray survey of the galactic plane by SAS-2 (Kniffen et al., 1973) several theoretical papers (Bignami and Fichtel, 1974; Puget and Stecker, 1974; Bignami et al., 1975; Stecker et al., 1975; Paul, Cassé and Cesarski, 1976) showed that the major features of the spatial distribution of high energy (> 100 MeV) γ-rays are well explained as the result of the decay of neutral pions produced by the interaction of energetic cosmic ray nucleons with the interstellar gas. Bignami et al. (1975), for instance, were successful in explaining not only the intensity, but the spatial distribution of the observed high energy emission. The basis of their model is the argument that, on the scale of galactic arms, the cosmic rays are concentrated in the vicinity of the spiral arms where the gas density, and hence the gravitational attraction, is greatest. The expected γ-ray intensity is then assumed to be the proportional to the product of the

cosmic-ray and matter densities along the line of sight. Details of the theoretical arguments supporting this model are discussed by Bignami et al. (1975) and by Kniffen et al. (1977). Fichtel et al. (1976) have pointed out that a logical conclusion from the model is that the bremsstrahlung emission of energetic cosmic ray electrons traversing this same interstellar matter would give rise to an emission that would be the dominant component in the total diffuse galactic emission below about 100 MeV. Subsequently Kniffen and Fichtel (1981) have shown that the Compton scattering of galactic visible and infrared photons by energetic cosmic ray electrons is also expected to be a major contributor to the observed medium energy diffuse emission. Using the infrared photon distribution of Boissé et al. (1981) and a stellar photon density based on the galactic stellar distribution model of Bahcall and Soneira (1980), these authors have derived the resulting γ-ray spectrum. Two major conclusions of this work were (1) that the contribution of Compton scattering component to the total diffuse galactic γ-ray emission from the central region of the galaxy is significantly greater than that resulting from bremsstrahlung emission, and (2) that the overall γ-ray spectrum is expected to be quite steep down to a few MeV with little indication of a π^0-decay feature at 67.5 MeV. An important test of the model is to extend the observations to lower energies. This was the objective of the observations to be reported here.

III. APPROACH

a) Detector

The instrument used in this experiment is a spark chamber γ-ray telescope which has been substantially modified from a detector used in 1975 to study γ-radiation at medium energies from the galactic center region (Kniffen et

al., 1978). Figure 1 shows a schematic view of the detector. The most important improvements in the new telescope system include 1) a time-of-flight directional telescope which has a lower threshold energy and much higher upward-moving rejection efficiency than the Cerenkov counters in the old detector; 2) high atomic number (tantalum) pair conversion foils which, compared to the aluminum plates, reduce the collisonal losses at comparable thickness measured in radiation length; 3) microprocessor controlled readout and on-board data system to decrease the dead time associated with transmitting events; and 4) a total energy scintillator and penetration counter to supplement information obtained from multiple scattering on event energies. Many of the technical details of the detector are described by Morris (1982).

A spark chamber stack assembly consisting of sixteen grids, interspersed with fifteen tantalum foils, constitutes the γ-ray imaging portion of the instrument. The dominant interaction process for γ-rays above 10 MeV in the foils is pair production. When such an interaction occurs, two charged particles issue from a common vertex within the stack and leave ion trails in the spark chamber gas. If triggered, the spark chambers provide two orthogonal, projected views of the electron and positron trajectories. Metal foils beyond the point of the pair production interaction serve as scattering material, and multiple Coulomb scattering theory and the trajectory information are used to estimate the energy of both pair members.

Two scintillator planes, separated by 40 cm, are located beneath the main spark chamber stack to determine the aperture of the detector. Charged particles produced by interactions in the spark chamber stack must penetrate both scintillator planes to provide a part of the requirements for an event trigger. Both planes are comprised of three optically isolated strips 16.8 cm

× 50.8 cm. Each strip is connected by light pipes whose elements are of equal length to photomultiplier tubes at each end. The photomultiplier tube signals are shared between the coincidence system and the time-of-flight system. The coincidence system requires nearly simultaneous signals from corresponding strips in the upper and lower plane. The time-of-flight measurement is compensated for the transit time of light along the scintillator-light-pipe paths by averaging the pulse arrival times from the photomultiplier tubes at opposite ends of each strip. Each digitized time-of-flight value below a commandable threshold provides a time-of-flight-good (TOFG) pulse to the coincidence system. Four additional spark grids, without pair conversion plates, are included between the scintillator planes to define the trajectories that produced the event trigger. Details of the entire time-of-flight system are given by Ross and Chesney (1980). Figure 2 shows the resolution of the time-of-flight system.

The total energy scintillator is 25 cm deep which corresponds to the range of an electron of 73 MeV. Since a portion of the radiative energy losses escape detection, the energy measured by this system is a lower limit value which is useful to supplement the information from multiple Coulomb scattering. The energy scintillator is viewed by eight photomultiplier tubes whose output signals are added. The energy detector, like the time-of-flight system, provides a signal to the coincidence circuit for events with energy greater than a commandable threshold. A large-area penetration counter is situated under the total energy scintillator to flag events where charged particles penetrate the energy counter.

The remaining counter is a 2.5 cm thick anticoincidence dome that surrounds the upper portion of the instrument to inhibit triggering on charged particle cosmic rays. Eighteen photomultiplier tubes, equally distributed about the lower edge, view the scintillator.

The coincidence system is commandable to four different modes, and in addition the thresholds for time-of-flight and total energy can be commanded. For this flight, the coincidence mode was set in a configuration which requires (1) a coincidence between the scintillator strips with an acceptable time-of-flight signal, (2) an energy deposited in the energy counter above a commandable threshold, (3) the absence of a signal in the anticoincidence dome and, (4) that the readout of the previous event has been completed.

The instrument was oriented in this flight at a fixed angle of 20° with respect to the zenith and was controlled azimuthally by a powered swivel in the load line to examine a commandable target direction . Output signals from a two axis magnetometer were converted on-board to a magnetic bearing. The address of the target bearing in a preloaded table was automatically incremented as a function of time by a microprocessor. In addition both the current target table address and the offset between magnetic and geographic bearing could be updated by the command system. The microprocessor then was able to compare the azmuthal pointing with the target value and to issue drive signals to the stepping motor on the power swivel. This system was capable of maintaining azimuthal pointing with ~ ± 0.5°.

b) Instrument Properties

The instrument area-efficiency and the accuracy to which it can determine event arrival angles and energy must all be known as functions of energy and arrival angle in the detector. In the analysis reported here, this information was obtained by a Monte Carlo computer program that has been developed and used on a variety of different detector designs over the past three years. This software system includes both pair-production and Compton processes for the γ-ray events, and for secondaries it includes multiple Coulomb scattering, collisional, and radiative energy losses in all elements

of the system. Moreover, events are screened by the same criteria used in dealing with actual data, namely two clearly distinct tracks (electron and positron) must issue from a common vertex located with the main spark chamber stack.

A γ-ray beam generated by in-flight annihilation of positrons was developed at the National Bureau of Standards linear accelerator (Bertsch and Dodge, 1981) and was used to calibrate the earlier configuration of this same detector. In this case, the Monte Carlo calculation agreed well with the observed data in terms of the energy and angular dependence of the angular resolution and area-efficiency. With this calibration, a normalization factor of 1.3 was applied to account for the uncertainty in the tagging efficiency of the calibration measurements and for other factors not taken into account in the Monte Carlo calculations. The old detector configuration, for instance, used a Cerenkov directional counter which was more difficult to model than the time-of-flight system. The SAS-2 instrument was also thoroughly calibrated at somewhat higher energies in a γ-ray beam, and the Monte Carlo program results were in close agreement with the experimental values without any normalization factors.

Figure 3a shows the relative number of γ-rays from the atmospheric and the galactic plane spectra together with the calculated area-efficiency for vertical incidence γ-rays. It is evident that the optimum energy region of the detector is from 10 to 100 MeV for the expected source spectrum. Angular resolution for vertical incidence is shown in Figure 3b. For off-axis directions this uncertainty increases approximately as the secant of the angle. Note that angular uncertainty in one dimension, for instance normal to the galactic plane, is smaller by a factor $1/\sqrt{2}$ than the cone angle uncertainty given here.

Because of the strip scintillator geometry, the area-efficiency function varies with azimuthal angle as well as with the polar angle of arrival. Figures 4a,b show the dependence of $A\varepsilon$ on θ, the angle with respect to the instrument axis, for several different energies and for the two extremes of azimuth. In practice, events with arrival angles where $A\varepsilon$ is less than 20% of its maximum (vertical incidence) value, or events with angles to the detector axis greater than 30° were excluded from analysis. These conditions define the useful aperture of the detector.

c) Flight

The balloon flight was conducted from Palestine, Texas, on September 24 and 25, 1980, using a balloon with volume 7.9×10^5 m^3. The total payload weight was 872 kg. The maximum altitude of 3.2 millibars was reached at 22:00 UT, but the depth increased slowly to 4.2 millibars by the end of data transmission, 8.6 hours later. The instrument performed well until 02:00 UT when it encountered a severe electrical storm that caused the orientation microprocessor to issue drive commands to false and variable targets. Attempts to reset the targets by command from the ground were only momentarily effective. Later in the flight when the weather improved, proper control was re-established. During the periods of bad orientation the aspect was changing so rapidly as to make the data impractical to interpret. Consequently, the analysis only includes good orientation time intervals for the float data; 22:43 UT to 02:10 UT, 02:45 UT to 03:08 UT, and 4:58 UT to 06:37 UT.

Several galactic longitude (ℓ) locations on the galactic plane ($b=0$) are shown in Figure 5 as a function of time as seen from Palestine, Texas at the date of the flight. The dotted curve shows the approximate aperture of the instrument in this projection for an aspect of 130° north bearing. For other aspects, this pattern simply shifts laterally on the plot. Aspect orientation

was controlled so as to maximize exposure to the lower galactic longitudes. This figure shows that the region of galactic plane that can be studied from the Texas latitude is $\ell > 20°$. Notice that the orientation of the galactic plane begins nearly normal to the longer dimension of the scintillator planes and changes with time to a more favorable alignment (parallel to the strips).

IV. ANALYSIS

a) Event Data

Gamma ray events that interact by pair production are uniquely distinguishable from background events by the "picture" of two tracks (e^+ and e^-) which issue from a common vertex. The most common types of background include separated single tracks that might occur from pair production interactions in the pressure vessel, Compton scattering interactions, occassional charged particles that escape detection by the anticoincidence dome or time-of-flight system (if upward moving), and showers from interactions in the spark chamber walls.

The first step in event data processing was done with a software system that screens the data from obviously bad events and then "structures" the picture by identifying sparks that are associated with tracks, and correlating the tracks in the two orthogonal views. A final stage of screening is then made to insure that the event represents a neutral primary that converts within the chamber volume into two charged secondaries.

All good events, and those that the computer could not decide clearly, were reviewed using a computer-interactive graphics device, and the analysis was modified as necessary. A sample of the events "clearly" rejected by the computer was also reviewed to insure that good data were not lost. The rejection rate was found to be completely negligible.

After the events were structured and reviewed, a multiple scattering analysis was made to estimate the energies of individual secondary particles. The γ-ray energy is simply the sum of the total energies of the secondary particle with a small correction for energy losses. Gamma-ray arrival directions were calculated from an energy-weighted average of the initial secondary track trajectories. The instrument also had a total energy scintillator (described earlier) however these results were not utilized in the analysis here because of a performance anomaly. Information on instrument location and aspect, the event arrival direction, and sidereal time was used to calculate the galactic coordinate of each γ-ray event, and skymap arrays in 5° × 5° bins in galactic coordinate space were produced for each of four energy bins; 10 to 30 MeV, 30 to 50 MeV, 50 to 80 MeV, and 80 to 200 MeV.

b) Gamma Ray Background

At the atmospheric depths of this flight and for the energy region considered, the principal background is expected to be due to cosmic ray interactions in the atmosphere. For the lowest energy region, 10 to 30 MeV, however, cosmic diffuse γ-rays are an important component. Lavigne et al. (1982) observed the diffuse cosmic γ-ray intensity to be $(4.8 \pm 1.9) \times 10^{-5}$ $\gamma/cm^2 sr$ sec MeV) between 10 and 25 MeV. This value is approximately 22% of the total background intensity in the same energy region at an atmospheric depth of 3.5 g/cm^2 (Kniffen et al., 1978). At higher energies the atmospheric contribution at 3.5 g/cm^2 completely dominates the cosmic contribution. Similar conclusions are obtained using the SAS-2 diffuse spectrum (Fichtel et al., 1977) extrapolated to 10 MeV. For depths less than 100 g/cm^2, the atmospheric background varies essentially linearly with depth (Thompson, 1974). Consequently the observed background varies within the detector aperture due to the large aperture size, the orientation of the detector at

20° from the vertical, and the angular dependence of instrument area-efficiency function. A good determination of this background is necessary for determining emission from the galactic plane.

In order to estimate the background, the sky was divided into a grid with 5° × 5° bins in galactic coordinates for the region $0 \leq \ell \leq 90°$ and $-40° \leq b \leq 40°$. The expected number of atmospheric background γ-rays within a given bin between energy limits E_1 and E_2 may be expressed as

$$N_{Bik}(E_1,E_2) = \int_t dt \int_{E_1}^{E_2} dE \left[\frac{dj}{dE}(E, p=1)\right]_B \int_{\ell_{ik}} d\ell \int_{b_{ik}} db \quad (1)$$

$$(\cos b)\ [A\varepsilon(E,\theta,\phi)]\ \frac{p(t)f(t)}{\cos z(\theta,\phi)}$$

where p is the atmospheric depth, $[dj/dE\ (E, p=1]_B$ is the atmospheric differential energy spectrum at unit depth, f(t) is the instrument live-time fraction which may vary with time t, ℓ_{ik} and b_{ik} denote the limits of the bin designated by subscripts i and k, θ and φ are the spark chamber polar and azimuthal angles, and z is the zenith angle corresponding to a given combination of θ and φ. At any given time the known instrument aspect angles, geographic location and local sidereal time are used to relate θ and φ to ℓ and b. Because of the limited energy and angular resolution of the detector already discussed, and the statistical uncertainty imposed by the small number of observed γ-rays, two approximations can be made to simplify eq. (1), namely, that for each of the four energy bins Aε can be evaluated at an average energy for that interval, and θ, φ, and z(θ, φ) can be determined at the centroid of each sky bin. Eq. (1) then reduces to

$$N_{Bik}(E_1,E_2) = J_B(E_1,E_2,p=1)\ S_{Bik}(\bar{E}) \tag{2a}$$

where

$$J_B(E_1,E_2,p=1) = \int_{E_1}^{E_2} dE\ \left[\frac{dj}{dE}\right]_B \tag{2b}$$

and

$$S_{Bik}(\bar{E}) = (\Delta\ell)(\Delta b)\ (\cos b_{ik}) \int\!\!\int dt\ \left\{A\varepsilon(\bar{E},\theta_{ik},\phi_{ik})\ \frac{f(t)p(t)}{\cos z(\theta_{ik},\gamma_{ik})}\right\} . \tag{2c}$$

Notice in calculating the atmospheric background exposure factors S_{Bik} at ℓ_{ik} and b_{ik} that θ_{ik} and ϕ_{ik} also depend on time since the instrument aspect and geographic location vary with time. For the grid mentioned, $\Delta\ell=\Delta b=5°$.

Atmospheric exposure factors $S_{Bik}(\bar{E})$ were evaluated for all bins and for each of the four energy ranges using time steps of 65.536 sec and by interpolating tabular data for aspect, live-time fraction, atmospheric depth, geographic location, and area-efficiency. Gamma rays that arrive from non-central portions of the sky map grid, in particular $|b|>10°$, were assumed to be due solely to the background. (See, e.g., Kniffen and Fichtel, 1981, for the latitude distribution of galactic plane emission.) In this portion of the sky, observed γ-ray counts and the calculated exposure factors were used in a least-squares procedure based on eq. (2a) to infer $J_B(E_1,E_2,p=1)$. Then using this result and the appropriate values of $S_{Bij}(\bar{E})$, the expected background counts were obtained for each bin in the central (galactic plane) region $|b|\leq 10°$. For the 10 to 30 MeV region where the cosmic γ-ray background is

important, the observed γ-ray counts in each bin were reduced by the expected diffuse contribution before the fitting process, and the assumed diffuse intensity was then added to $J_B(E_1, E_2, p=1)$ to get the total background. Here the diffuse component was estimated using the Lavigne et al. (1982) observation and exposure factors, similar to eq. 2C except without the factors p(t) and cos $z(\theta_{ik}, \gamma_{ik})$ which are not appropriate for cosmic sources. Finally, the total background intensity determined for data from $|b|>10°$ was used with appropriate values of $S_{Bij}(\overline{E})$ to estimate the background counts in each bin in the central (galactic plane) region $10°<|b|$.

c) Galactic Plane Gamma Rays

Arguments similar to those given for developing eqs. (2a,b) can be given for galactic plane radiation, except here the source spectrum does not depend on atmospheric depth (Absorption has a negligible effect on the energy spectrum at the residual pressure of this flight.) and the galactic plane, having a source region thin compared to the angular resolution of the instrument, is treated as a line source. In the case

$$N_{Gij}(E_1,E_2) = J_G(E_1,E_2)\ S_{Gij}(E) \tag{3a}$$

where

$$J_G(E_1,E_2) = \int_{E_1}^{E_2} dE\left(\frac{dj}{dE}\right)_G \tag{3b}$$

and

$$S_{Gij}(E) = (\Delta\ell)\cos b_{ij} \int dt \left\{A\varepsilon(E,\theta,\gamma)f(t)\right\} . \tag{3c}$$

The function J_G has units of (area × time × angle)$^{-1}$ while J_B has units of (area time × solid × angle)$^{-1}$ and the S functions differ by one unit of angle as well. Finally the galactic flux is determined from a fit to eq. (3a) using calculated values S_G and the difference between observed counts and expected counts for each bin.

V. RESULTS

The background γ-ray intensities in each of the four energy intervals were determined by the procedure described above. These results are shown in Figure 6 along with data from several other experiments. All values were scaled to a residual depth of 3.5 g/cm^2 assuming that the background is dominated by the atmosphere so that it depends linearly on depth in the range of interest here. The results of Kniffen et al. (1978) were obtained with the earlier version of the present detector at a geomagnetic cutoff of 11.2 GV and were also scaled to 4.5 GV using a factor of 1.0/0.57 suggested by Staib et al. (1974). The good agreement between the background measurement in this experiment and most of the other results is confirmation that the calculated experiment efficiencies are accurate over the energy interval of interest. These efficiences enter into the background and source exposure factors in the same manner (eqs. 2c and 3c).

The fitted background intensities and background sensitivities for the skybins centered on the galactic plane were used to estimate the number of background γ-rays as a function of galactic longitude. These results are shown as dotted lines in Figures 7a,b,c together with the total number of γ-rays (solid lines) recorded in the same bins. For the two lower energy regions, 10 to 30 MeV and 30 to 50 MeV, counts were summed over the latitude interval $|b| < 10°$ which includes two standard deviations of the angular

uncertainty of the detector and its orientation uncertainty during flight. The region was reduced to $|b| < 5°$ at the higher energies because the angular resolution of the detector improves with energy. In Figures 7d,e,f the difference between observed and expected background γ-rays are shown by the solid lines for the same energy regions as the plots immediately above each figure. The dashed lines in the bottom row of plots in Figure 7 show the difference between observed and expected background in the regions immediately off the galactic plane, $10° < |b| < 20°$ in Figure 7d,e and $5° < |b| < 10°$ in Figure 7f. For all three energy intervals an excess of γ-rays is observed for the galactic plane in the longitude interval $20° < \ell < 45°$. A relative likelihood method (Hearn, 1969) was used to evaluate confidence levels of 96.8%, 93.2%, and 95.7% for the excess events in the energy intervals 10 to 30 MeV, 30 to 50 MeV and 50 to 80 MeV. Above 80 MeV the observed number of γ-rays was too small to give a significant excess. Notice that the off-plane results do not show a significant excess. At galactic longitudes below 20° the instrument sensitivity rapidly approaches zero since this portion of the plane is near the limit of the aperture (see Figure 5) and is far from the zenith so that atmosphere background is relatively large. Above longitude 45° the galactic plane emission apparently decreases significantly (Hartman et al., 1974).

The exposure factors of the detector for galactic plane emission for the 5° x 5° skybins in the regions of enhancement were evaluated as described in the previous section and were used along with the excess γ-rays in Figure 7 to evaluate the galactic plane intensities in the region from 10 to 80 MeV shown in Figure 8. These results are compared with observations from other experiments for similar regions of the galactic plane. The solid curve is the calculated spectrum by Fichtel and Kniffen, 1982.

Finally, the spectral data from medium and high energy γ-ray measurements are compared with results from X-ray and low energy γ-ray studies in Figure 9. Clearly the extrapolated curve from the results in the 10 to 100 MeV region to lower energies falls above observations in the 100 keV to 4 MeV region, yet is consistent with the data below ~ 50 keV.

VI. CONCLUSION

The results obtained in this work have been obtained with an improved medium energy spark chamber γ-ray detector, which extends the reliable detection of γ-rays by pair production down to about 10 MeV. The good overall agreement between several observations in the atmospheric intensities and spectrum establish a new level of confidence in the results. The galactic γ-ray spectrum obtained, especially in the medium energy range, is now believed to be solidly established. The remaining statistical uncertainties can only be reduced by additional observations either by southern hemisphere balloon exposures, or more definitively by shuttle or satellite observations.

The implications of the current work establish (1) that the steep spectral slope in the medium energy γ-ray range continues down to at least 10 MeV and (2) that the electron spectrum inferred from the γ-ray spectrum is consistent with recent theoretical predictions (Fichtel and Kniffen, 1982). The latter point is particularly important because the interstellar electron spectrum in the region below a few hundred MeV cannot be directly observed in the solar vicinity because of solar modulation effects. This conclusion must be drawn with caution, however, because the emission is believed to be primarily the result of the bremsstrahlung interactions of energetic cosmic-ray electrons with the interstellar gas. The intensity thus depends upon the product of the cosmic-ray electron and interstellar gas densities, and neither is well established.

The theoretical model (Fichtel and Kniffen, 1982) assumes proportionality between the cosmic ray electron and interstellar gas densities, an assumption which gives good agreement with both the high and medium energy observations, both in spectral shape and in spatial distribution. The hope for a more definitive separate determination of the cosmic ray and interstellar gas densities depends on future observations with better precision which will allow separation of the elements by studying the detailed spectral and latitude dependencies (Kniffen and Fichtel, 1981) of the galactic diffuse γ-ray emission over a wide range of energies.

As seen in Figure 9 the data from 10 to about 200 MeV are consistent with a power law spectrum. When extended to the 6-350 keV data of Wheaton (1976) the fit is remarkably good considering the range of the extrapolation. In the 0.1 to 4 MeV range, however, there are clearly data which fall well below the extrapolated power law. Matteson (1982) has summarized many galactic center observations in the hard X-ray to low energy γ-ray region pointing out the apparent strong time variability in the low energy γ-ray region, characterized as a power law spectrum with variable slope. The hard X-ray data shows the least variation in intensity, with a greater variation at the low energy γ-ray energies. The suggestion is that variability is caused by an intense, variable source at the galactic center which is unresolved in most of the observations. If this is the case, the spectral break at a few MeV might imply the transition from predominantly diffuse processes at the high energies to a spectrum influenced by a variable discrete source or sources in the hard X-ray low energy γ-ray region. However, the conclusion must be made with caution because of the different properties of the instruments and the regions of the central galactic region explored. Further observations with good spatial resolution are needed to verify this conclusion in this very difficult observation portion of the spectrum.

REFERENCES

Agrinier, B., Bonfand, E., Parlier, B., Gros, M., Lavigne, J.M., Neil, M., and Rao, K.R. 1981, 17th Internat. Cosmic Ray Conf., 9, 72.

Bahcall, J.N. and Soneira, R.M. 1980, Ap. J. (Letters), 238, L17.

Bertsch, D.L. and Dodge, W.R. 1981, Nucl. Instr. Methods, 185, 439.

Bignami, G.F. and Fichtel, C.E. 1974, Ap. J. (Letters), 189, L65.

Bignami, G.F., Fichtel, C.E., Kniffen, D.A., and Thompson, D.J. 1975, Ap. J., 199, 54.

Boissé, P., Gispert, R., Coron, N., Wijnbergen, J., Serra, G., Ryter, C., and Puget, J.L. 1981, Astr. Ap., 94, 265.

Fichtel, C.E., Hartman, R.C., Kniffen, D.A., Thompson, D.J., Bignami, G.F., Ögelman, H., Özel, M.E., and Tümer, T. 1975, Ap. J., 198, 163.

Fichtel, C.E., Hartman, R.C., Kniffen, D.A., Thompson, D.J., Ögelman, H.B., Özel, M.E., and Tümer, T. 1977, Ap. J. (Letters), 217, L9.

Fichtel, C.E. and Kniffen, D.A. 1982, "A Study of the Diffuse Galactic Gamma Radiation", to be published in the Proceedings of the International Workshop on Very High Energy Gamma Ray Astronomy, Octacamund, India, Sept. 20-25 (NASA TM 83992).

Fichtel, C.E., Kniffen, D.A., Thompson, D.J., Bignami, G.F., and Cheung, C.Y. 1976, Ap. J., 208, 211.

Gilman, D., Metzger, A.E., Parker, R.H., and Trombka, J.I. 1979, Ap. J., 229, 753.

Hartman, R.C., Kniffen, D.A., Thompson, D.J., Fichtel, C.E., Ögelman, H.B., and Tümer, T. 1979, Ap. J., 230, 597.

Hearn, D. 1969, Nucl. Instr. Methods, 70, 200.

Kinzer, R.L., Share, G.H., and Seeman, N. 1974, J. Geophys. Res., 79, 4567.

Kniffen, D.A., Bertsch, D.L., Morris, D.J., Palmeira, R.A.R., and Rao, K.R. 1978, Ap. J. 225, 591.

Kniffen, D.A. and Fichtel, C.E. 1981, Ap. J. 250, 389.

Kniffen, D.A., Fichtel, C.E., and Thompson, D.J. 1977, Ap. J., 215, 765.

Kniffen, D.A., Hartman, R.C., Thompson, D.J., and Fichtel, C.E. 1973, Ap. J. (Letters), 186, L105.

Lavigne, J.M., Niel, M., Vedrenne, G., Agrinier, B., Bonfand, E., and Parlier, B. 1982, Ap. J., 261, 720.

Mandrou, P., Bui-Van, A., Vedrenne, G., and Niel, M. 1980, Ap. J., 237, 424.

Matteson, J.L. 1982, Proceedings of AIP Conference No. 83 on the Galactic Center, Eds. G.R. Riegler and R.D. Blandford, 109.

Mayer-Hasselwander, H.A., et al. 1980, Ann. N.Y. Sci., 336, 211.

Mayer-Hasselwander, H.A., et al. 1982, Astron. Astrophys., 105, 164.

Morris, D.J. 1982, Ph. D. Thesis, University of Maryland.

Paul, J., Cassé, M., and Cesarsky, C.J. 1976, Ap. J., 207, 62.

Puget, J. and Stecker, F.W. 1974, Ap. J., 191, 303.

Ross, R.W. and Chesney, J.R. 1980, IEEE Trans. on Nucl. Sci., NS-27, #1, 370.

Ryan, M., Moon, S.H., Wilson, R.B., Zych, A.D., and White, R.S. 1977, 15th Internat. Cosmic Ray Conf. (Plovdiv: Bulgarian Academy of Science), 1, 73.

Schönfelder, V., Graser, U., and Daugherty, J. 1977, Ap. J., 217, 306.

Staib, J.A., Frye, G.M., and Zych, A.D. 1974, J. Geophys. Res., 79, 929.

Stecker, F.W., Solomon, P.M., Scoville, N.Z., and Ryter, C.E. 1975, Ap. J., 201, 90.

Thompson, D.J. 1974, J. Geophys. Res., 79, 1309.

Wheaton, W.A. 1976, Ph. D., Thesis, USCD (SP 76-01).

FIGURE CAPTIONS

Figure 1: Schematic view of the medium energy γ-ray telescope

Figure 2: Time-of-flight distribution. In these histograms each channel corresponds to a time interval of 190 picoseconds. Spectrum (a) was accumulated using ground level muons prior to flight with the anticoincidence disabled and with the instrument upright and inverted for equal intervals of time. Downward and upward moving events are separated at approximately channel 27. Spectrum (b) was obtained with charged particles and neutral events at float altitude. Here the downward component clearly dominates. Spectrum (c) is obtained with neutral events (primarily γ-rays) at float altitude. The decrease in resolution results from the multiple tracks in a γ-ray pair conversion which affect the time compensation of the time-of-flight system. The threshold of channel 25 was used to trigger on downward-moving γ-rays in flight.

Figure 3: The relative detection rates for galactic and atomspheric γ-rays and the area-efficiency and angular resolution as functions of energy for the detector. The relative rates in (a) are based on spectra reported by Kniffen et al. 1978 and are included here to show that even though the area-efficiency does not reach maximum until ~ 100 MeV, the most probable event energy occurs at ~ 15 MeV. The relative rates are determined for an atmospheric depth of 3.4 g/cm^2 at 4.5 GV and using the cone of angular uncertainty which varies with energy. The atmospheric component is ~ 2 times greater than the galactic component. The rms angular

uncertainty in (b) should be reduced by $1/\sqrt{2}$ for the uncertainty in one dimension.

Figure 4: The Monte-Carlo calculated instrument detection efficiency as a function of energy and the angle from the detector axis. The two figures contrast the two azimuthal extremes in the efficiency of the detector. This variation arises from the time-of-flight scintillator geometry (see text).

Figure 5: Transit of selected positions on the galactic plane as observed during the balloon flight. The instrument was tilted 20° with respect to the zenith and controlled azimuthally. The dotted lines show the approximate aperture of the detector for an azimuth bearing of 130°. For other pointings the aperture profile moves laterally on this figure. Pointing was controlled to optimize exposure to the lower galactic longitudes. For longitudes below 20° the exposure to the galactic plane approaches zero.

Figure 6: Total gamma ray energy distribution obtained with this experiment compared with other experiments. Galactic plane regions were excluded from this analysis. The all-sky diffuse γ-ray contribution is expected to be small compared to the atmospheric spectrum at the depth of 3.5 g/cm^2 so that these results are essentially atmospheric.

Figure 7: Distribution of γ-ray events with galactic longitude for (a and d) 10 to 30 MeV, (b and e) 30 to 50 MeV, and (c and d) 50 to 80 MeV. In (a) and (b) the curve denotes the total number of observed γ-rays on the galactic plane $|b| < 10°$ and the dotted line is the expected background. (See text for details.) For

(c) the same convention applies but the plane interval is narrowed to $|b| < 5°$ since the angular resolution is beter at high energies. The bottom row of figures correspond to the same energy intervals as the figures immediately above them, but here the solid lines represent the excess γ-rays from the plane region. The dotted curves in (d and e) are excess γ-rays in an equivalent latitude interval off the galactic plane, $10° < |b| < 20°$ while in (f) the dotted curve is the excess in $5° < |b| < 10°$. In all three energy ranges, excess counts between $20 < \ell < 45°$ are found with the following significance: (d) 96.8%, (e) 93.2%, and (f) 95.7%.

Figure 8: Galactic plane gamma ray energy distribution in the medium and high energy regions. Data from this experiment are determined from galactic longitudes $20 < \ell < 45°$. Longitude intervals of other experiments are Agrinier et al. ($330° < \ell < 30°$, Kinzer et al. ($350° < \ell < 35°$), Mayer-Hasselwander et al. ($20° < \ell < 45°$), Hartman et al. ($355° < \ell < 30°$), and Kniffen et al. ($340° < \ell < 30°$). The solid curve is calculated by Fichtel and Kniffen (1982) at $\ell = 330°$, but essentially the same result is obtained at longitudes of this observation (private communication).

Figure 9: Comparison of the galactic plane energy distribution between medium and high energy γ-rays and emission at lower energies. The solid curve is the calculated distribution from Fichtel and Kniffen (1982) and the large-dashed line is an extrapolation of this curve to lower energies. The small-dashed curve, is the approximate fit to the observed data in the range from 10 keV to 1 MeV.

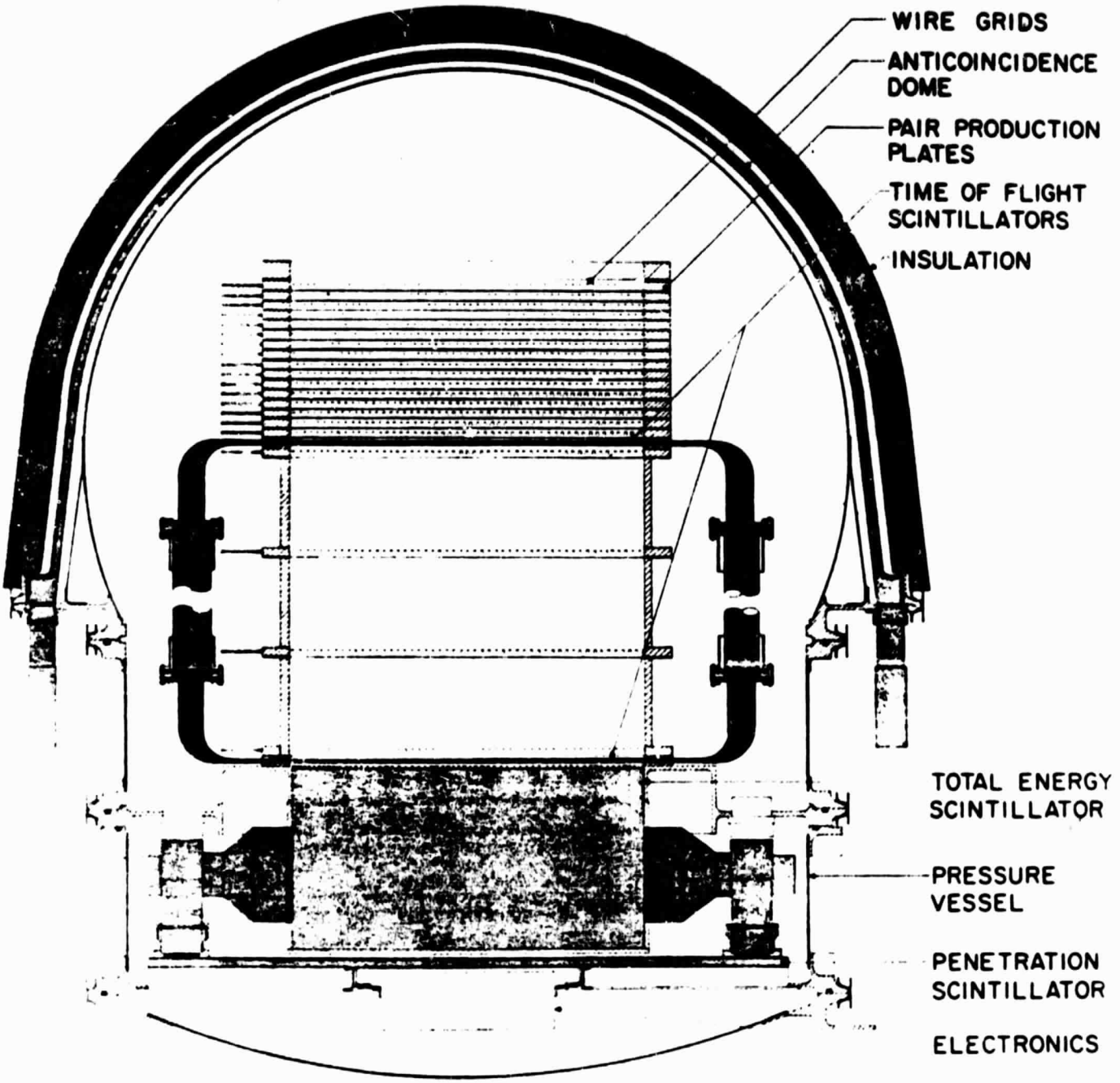

Figure 1

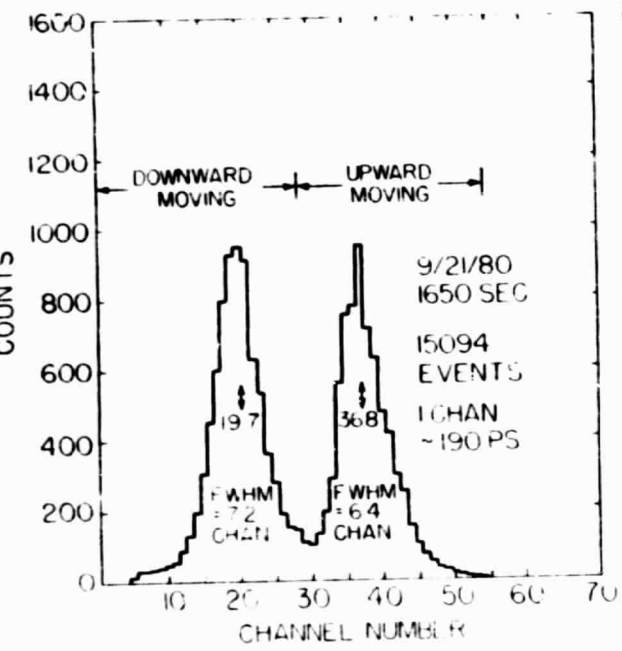

Figure 2a

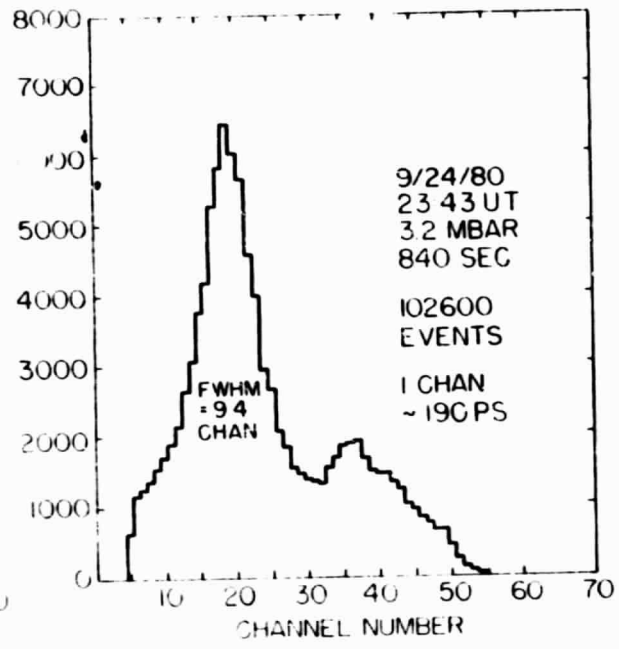

Figure 2b

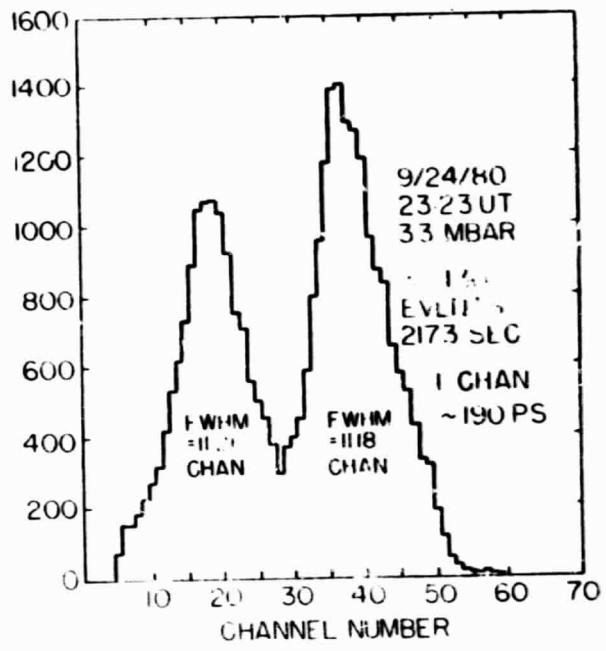

Figure 2c

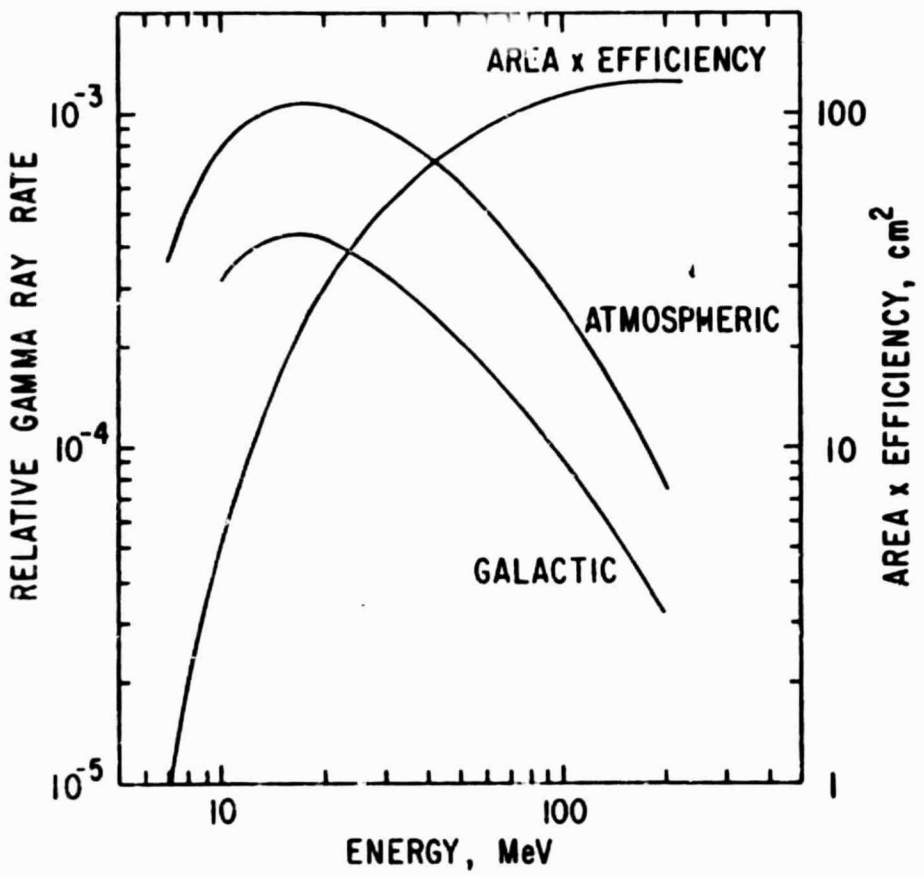

Figure 3a

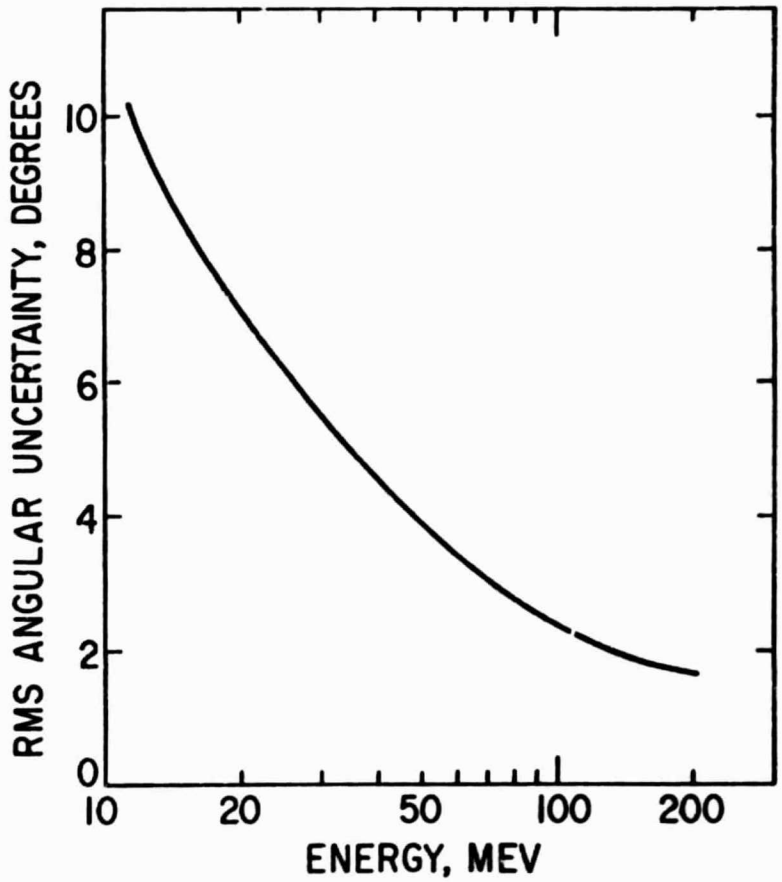

Figure 3b

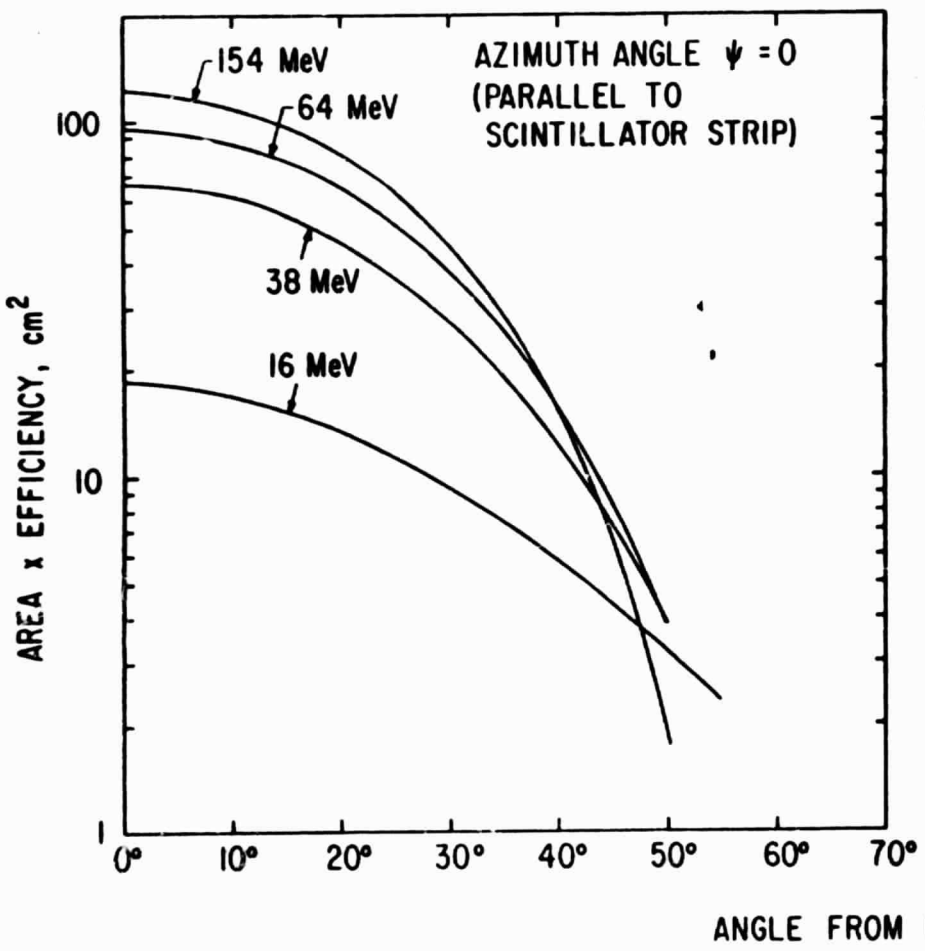

Figure 4a

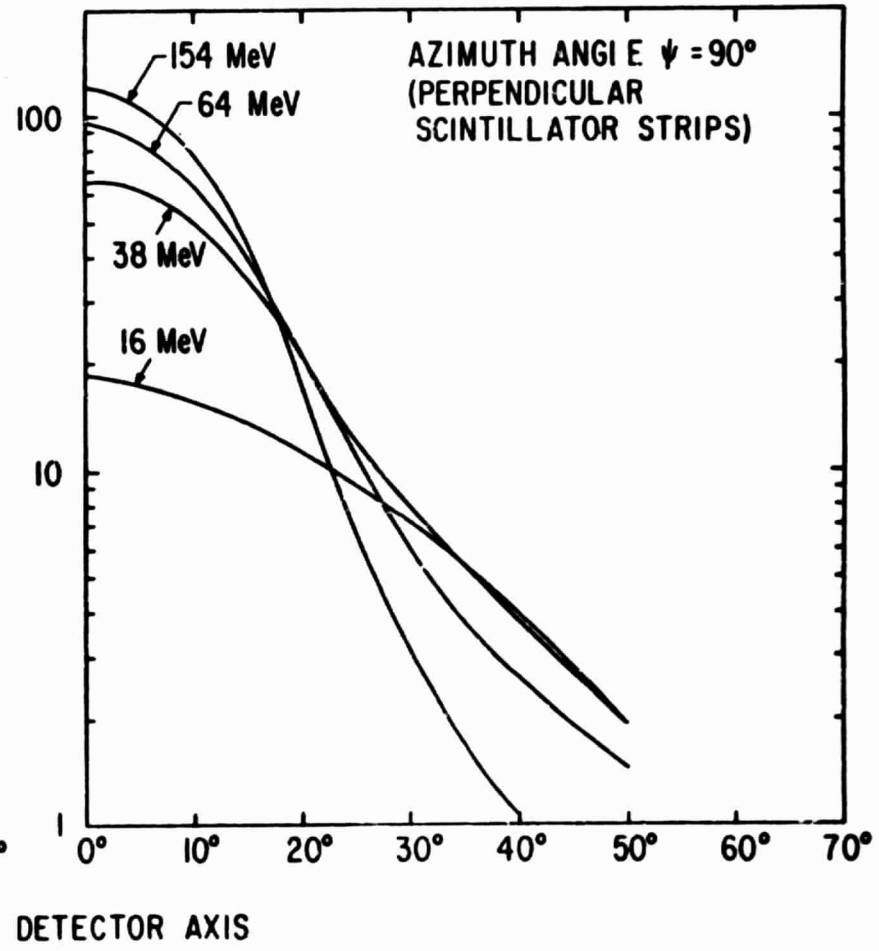

Figure 4b

AREA x EFFICIENCY, cm^2

ANGLE FROM DETECTOR AXIS

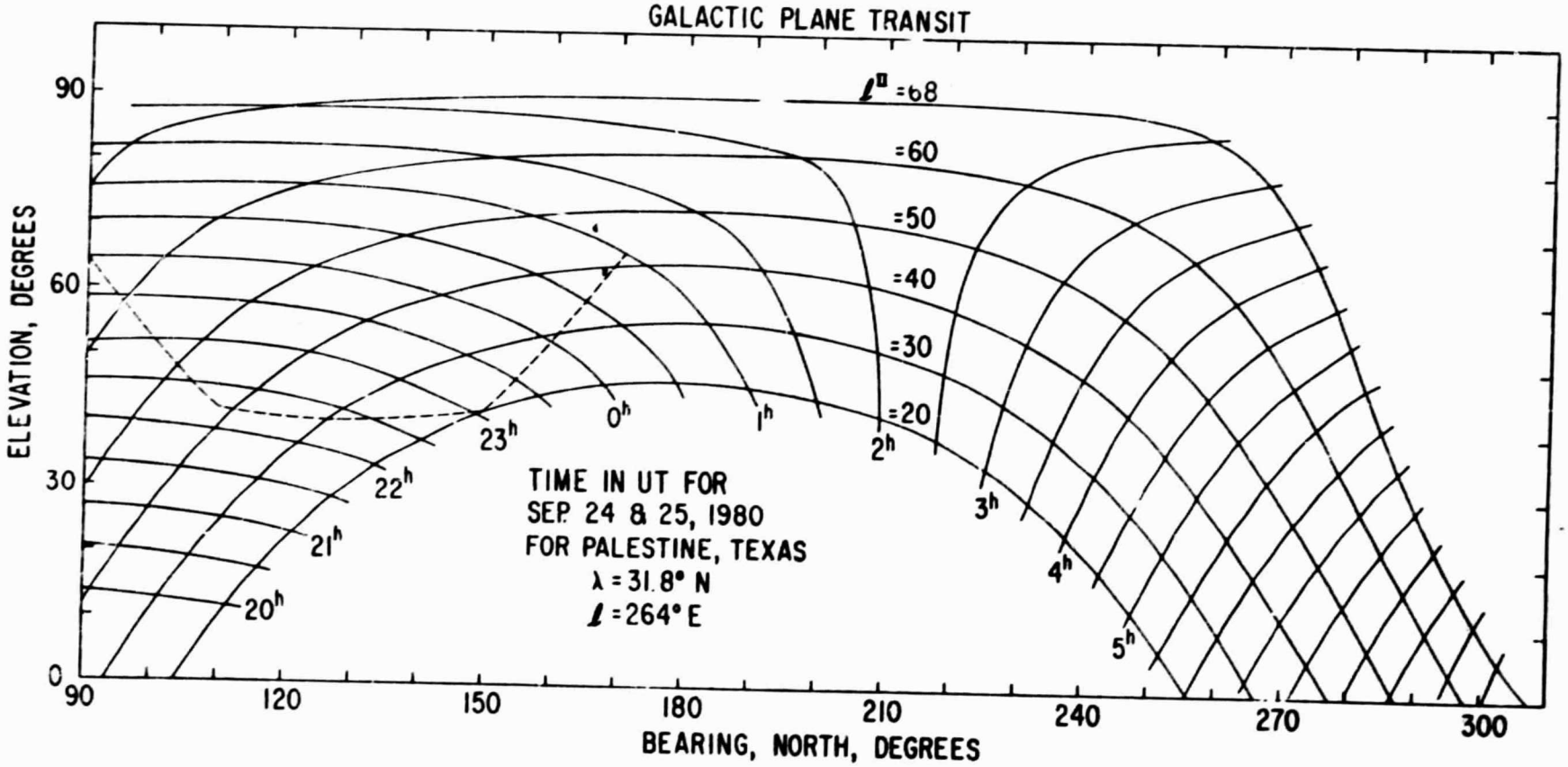

ORIGINAL PAGE IS
OF POOR QUALITY

Figure 5

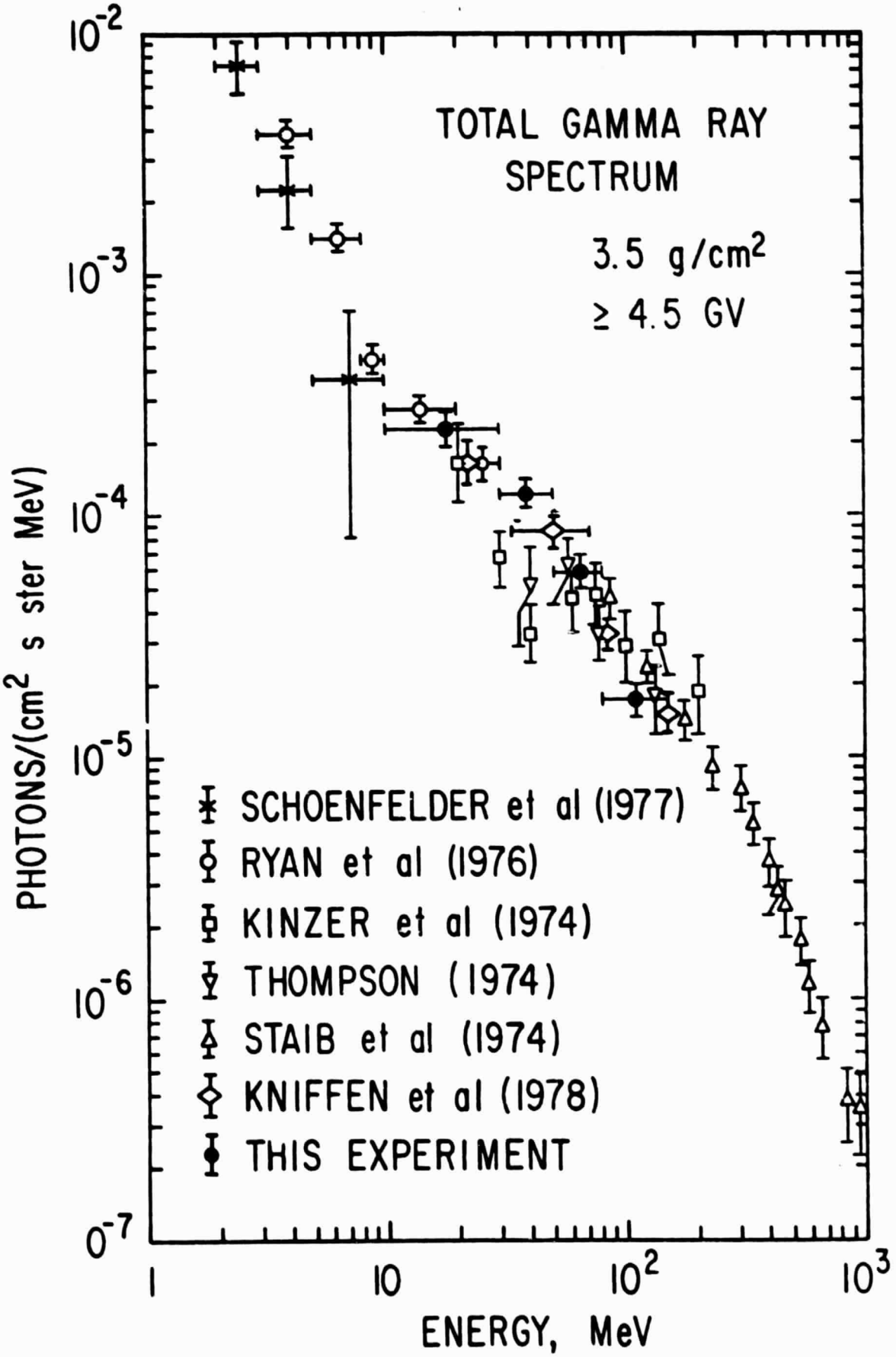

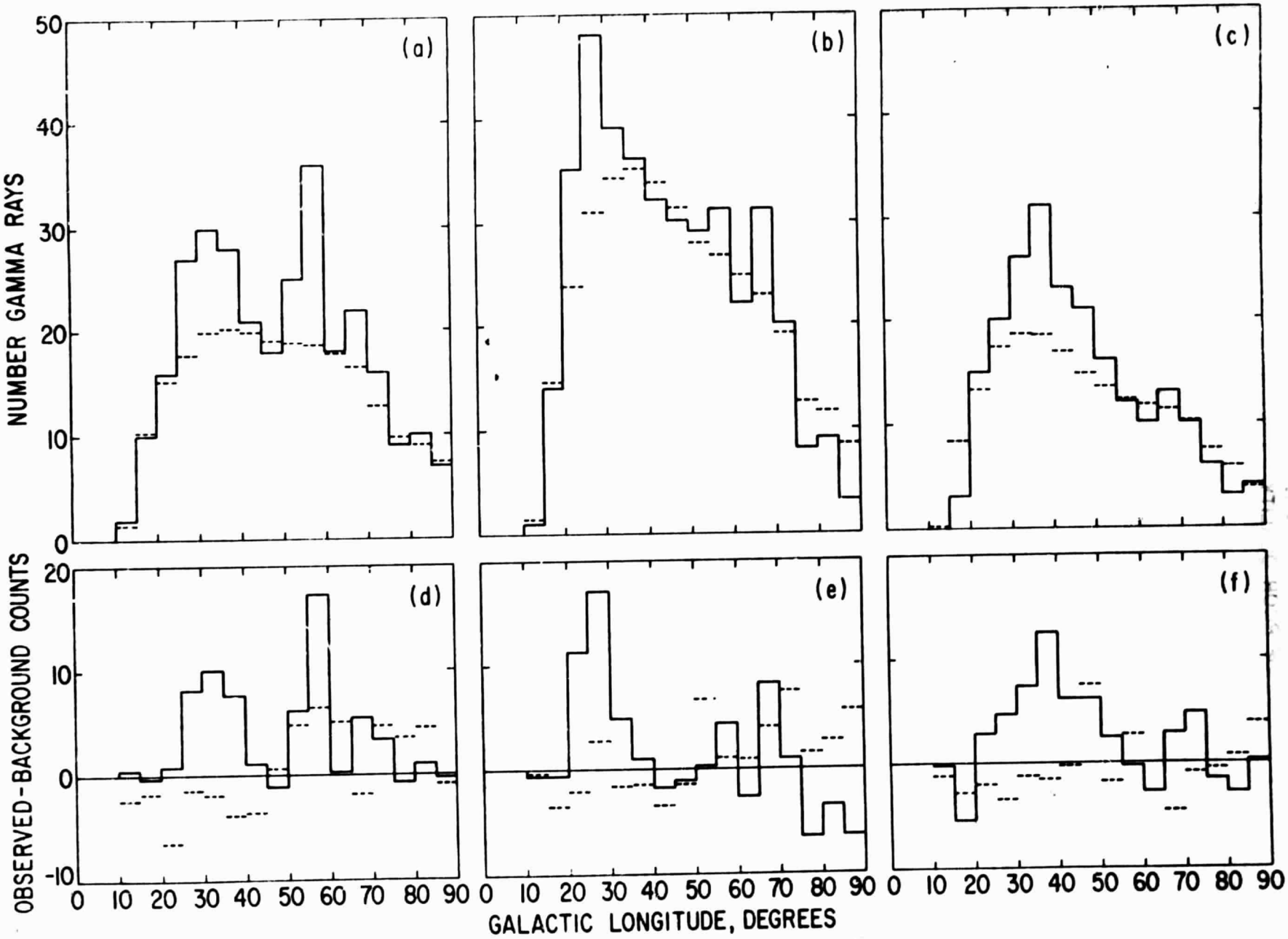

Figure 7

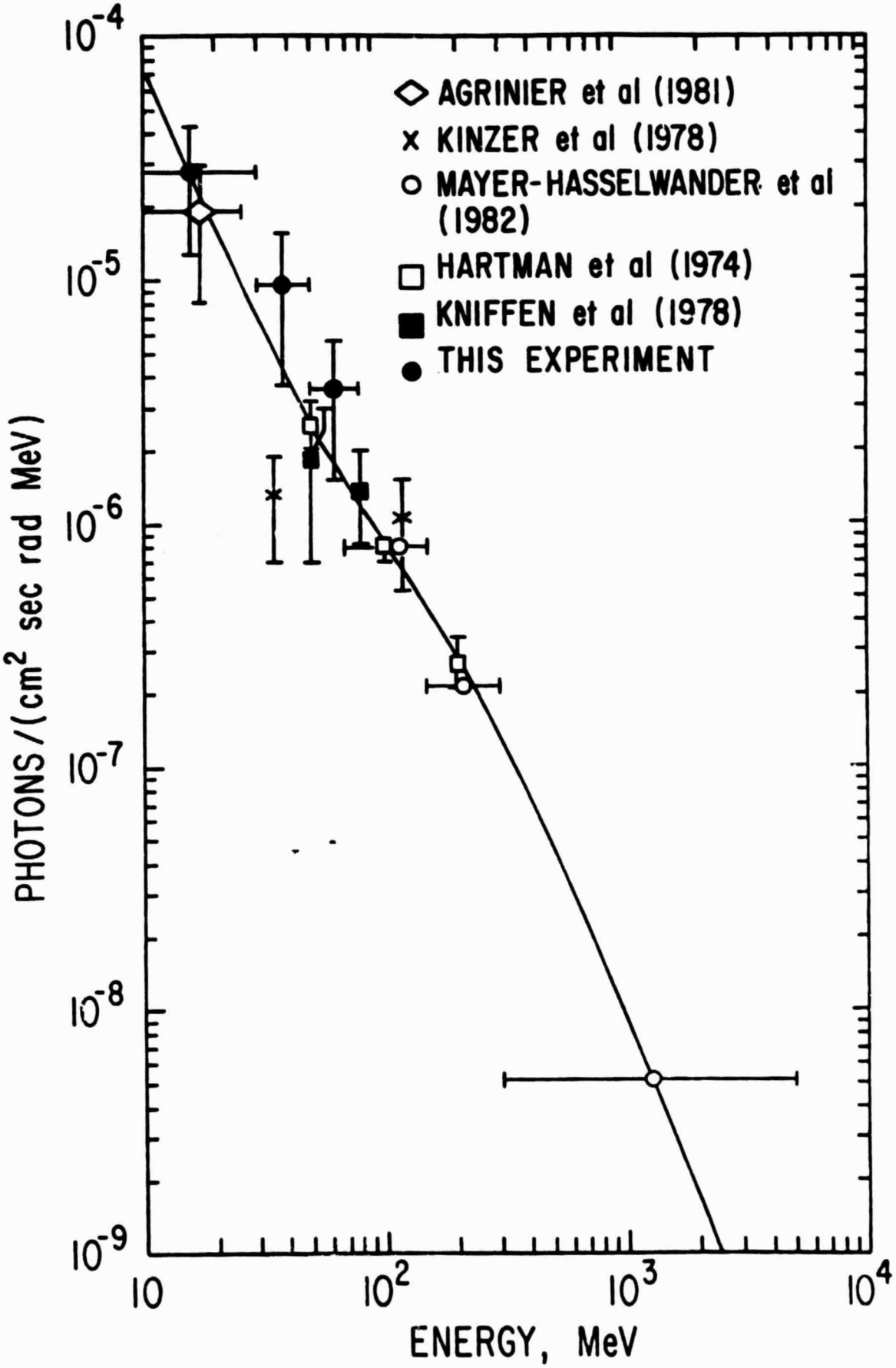

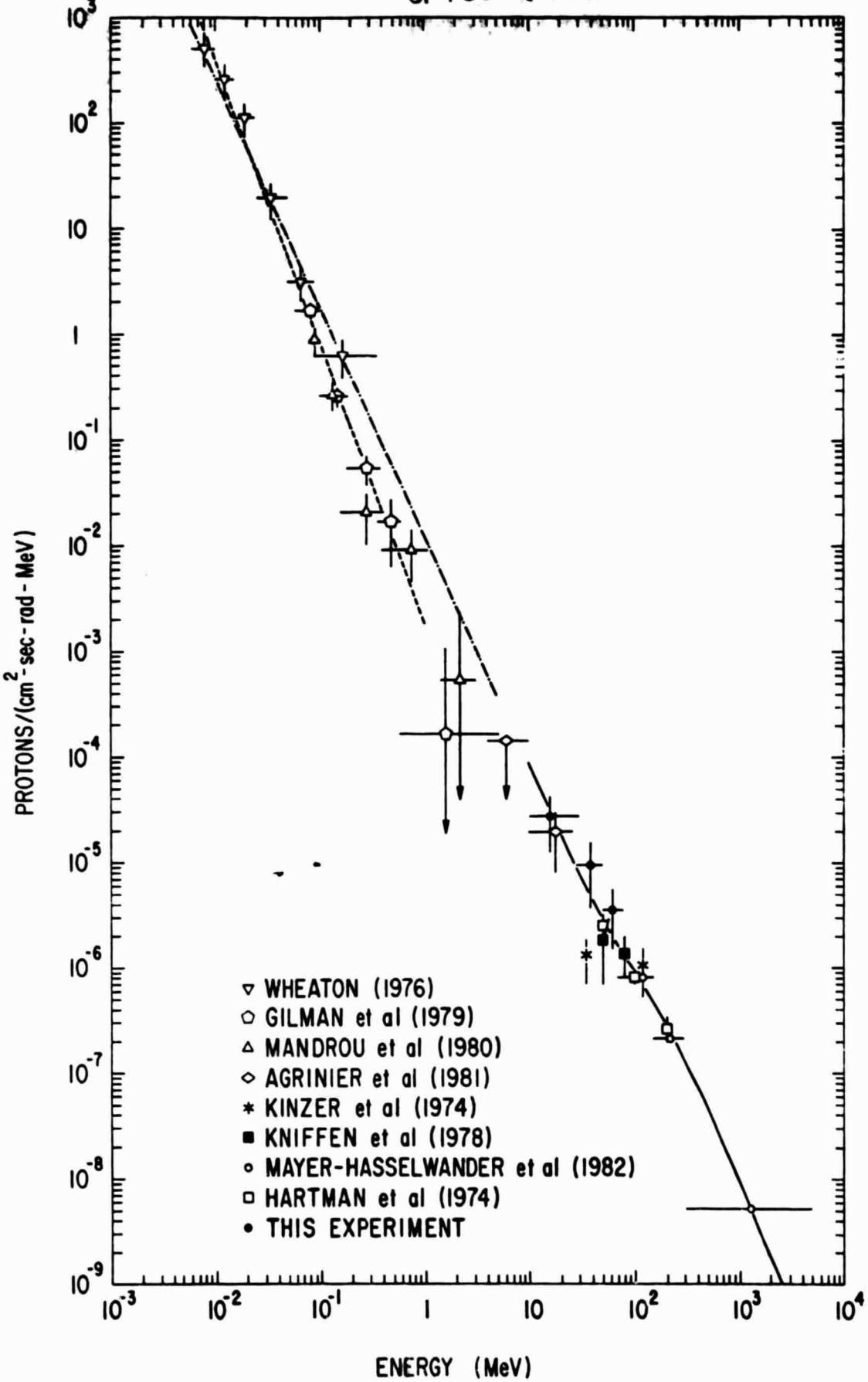

Figure 9